This article has been accepted for publication in a future issue of this journal, but has not been fully edited. Content may change prior to final publication. Citation information: DOI 10.1109/TII.2019.2935246, IEEE Transactions on Industrial Informatics

Observer-Driven Charging of Supercapacitors

Heng Li, *Member, IEEE*, Jun Peng, *Member, IEEE*, Jianping He, *Member, IEEE*, Zhiwu Huang, *Member, IEEE*, and Jing Wang, *Senior Member, IEEE*

***Abstract*—Cell balancing is crucial for charging supercapacitor cells to prevent cells from over-charging. Most existing cell-balancing charging methods typically adopt an output feedback control, i.e., the terminal voltages of cells are directly utilized in the controller design. One limitation of these methods is the voltage drop effect when the charging is terminated, which degrades the system capacity and results in cell imbalance. To address this challenge, in this paper, we propose an observer-driven charging method for supercapacitors. The switched resistor circuit is applied and is further modeled using the switched systems theory, where the RC model of cells is considered. The communication interactions among cells is modeled using the graph theory. A switching Luenberger observer is designed to estimate the voltage of the equivalent capacitor of each cell, and a consensus-based switching control law is designed to charge and balance supercapacitors. The closed-loop system model is derived using the block diagram. A laboratory testbed has been built to verify the effectiveness of the proposed charging method. Experiment results show that the proposed method can effectively alleviate the voltage drop effect when compared with existing charging methods.**

***Index Terms*—Supercapacitors; Consensus; Charging; Observer**

NOMENCLATURE

$v_{ck} = x_k$	The equivalent capacitor voltage (state variable) of cell k.
$v_k = y_k$	The terminal voltage (output variable) of cell k.
$i_c = u$	The charging current from power source (control input).
r_k	The equivalent-series-resistor (ESR) of cell k.
C_k	The capacitance of cell k.
R	The resistance of balancing resistors.
s_k	The on/off of cell k's switch.
σ_k	The σ_kth mode of cell k.
$A_k^{\sigma_k}$	The state parameter of cell k under mode σ_k.
$B_k^{\sigma_k}$	The input parameter of cell k under mode σ_k.
$C_k^{\sigma_k}$	The output parameter of cell k under mode σ_k.
$D_k^{\sigma_k}$	The transition parameter of cell k under mode σ_k.
x_0	The reference voltage.
$\zeta_k^{\sigma_k}$	The observer gain of cell k under mode σ_k.
$\hat{x}_k$	The estimation of x_k.
$\hat{y}_k$	The estimation of y_k.
δ_k	The tracking error of cell k.
e_k	The estimation error of cell k.
$\mathbf{L}$	The Laplacian matrix of the graph.
$\mathbf{G}$	The pinning matrix of the graph.
$\mathbf{D}$	The degree matrix of the graph.
$\mathbf{X}$	The state variable vector.
$\mathbf{Y}$	The output variable vector.
$\boldsymbol{\Delta}$	The tracking error vector.
$\mathbf{E}$	The estimation error vector.
$\boldsymbol{\sigma}$	The mode vector.
$\hat{\mathbf{X}}$	The state estimation vector.
$\hat{\mathbf{Y}}$	The output estimation vector.
$\mathbf{A}^{\boldsymbol{\sigma}}$	The state matrix.
$\mathbf{B}^{\boldsymbol{\sigma}}$	The input matrix.
$\mathbf{C}^{\boldsymbol{\sigma}}$	The output matrix.
$\mathbf{D}^{\boldsymbol{\sigma}}$	The transition matrix.
$\boldsymbol{\zeta}^{\boldsymbol{\sigma}}$	The observer gain matrix.

This work is partially supported by National Natural Science Foundation of China (Grant Nos. 61803394, 61672537, 61773257 and 61772558), Hunan Provincial Natural Science Foundation of China (Grant No. 2019JJ50822). (*Corresponding Author: Zhiwu Huang*)

Heng Li and Jun Peng are with School of Computer Science and Engineering, Central South University, Changsha, China, 410083 (email:{liheng, pengj}@csu.edu.cn).

Jianping He is with Department of Automation, Shanghai Jiao Tong University, and Key Laboratory of System Control and Information Processing, Shanghai, China 200240 (email: jphe@sjtu.edu.cn).

Zhiwu Huang are with School of Automation, Central South University, Changsha, China, 410083 (email: hzw@csu.edu.cn).

Jing Wang is with Electrical and Computer Engineering, Bradley University, Peoria, IL, USA 61625 (email: jingwang@bradley.edu).

I. INTRODUCTION

SUPERCAPACITORS have attracted growing interests in industrial applications owing to their superiorities over traditional batteries in certain aspects, e.g., high power density and extremely long lifetime [1]–[3]. Due to the high power rates, supercapacitors are especially welcome in the transportation electrification field, where frequent charging and discharging occur, e.g., they can be used as a buffer in hybrid energy storage systems of electric vehicles [3], or used as the main power source for urban rail vehicles [4].

Similar to conventional batteries, in the charging of supercapacitors, cell balancing circuits are typically required to balance the voltages of cells and prevent cells from over-charging [5]–[7]. The voltage imbalance is mainly caused by the manufacturing tolerance and uneven temperature distribution during operation. The imbalance is further deteriorated by uneven state-of-health (SoH) degradations of cells [7]. Two categories of balancing circuits have been proposed in the literature [7], [8], i.e., active balancing circuits [9], which transfer energy from high-voltage cells to the low-voltage ones, and passive balancing circuits [10], [11], which dissipate the energy of high-voltage cells on passive components, e.g., resistors. Specifically, switched resistor circuit is a widely-used passive balancing circuit in practice [7].

The decentralized cell balancing method is a classical approach for supercapacitor energy storage systems with switched resistor circuits [8]. In the decentralized cell balancing method, the switch is turned on when the cell voltage

This article has been accepted for publication in a future issue of this journal, but has not been fully edited. Content may change prior to final publication. Citation information: DOI 10.1109/TII.2019.2935246, IEEE Transactions on Industrial Informatics

is larger than the reference voltage, and vice versa. Due to the lack of coordination among cells, the cells that have been fully charged have to turn on the switches and shunt the charging current to balancing resistors to wait for the other cells to be fully charged. However, it is typically difficult to totally shunt the charging current to resistors due to charging current variations and resistance deviation, resulting in voltage swells and overcharging of cells during the charging process.

Consensus-based cell balancing approach has been an effective method to address the voltage swell problem of supercapacitors during the charging process [11]. The basic idea is that the switch of each cell is regulated by comparing the cell's voltage with those of its neighbors to synchronize cell voltages before cells are fully charged. Then, there is no need to shunt the charging current to balancing resistors, and the voltage swells and overcharging of cells can be avoided during the charging process.

However, existing consensus-based cell balancing methods suffer from the voltage drop effect when the charging is terminated. This is because the equivalent-serial-resistors (ESRs) of cells are neglected in the charging controller design, which leads to a voltage drop of ESRs when the charging is terminated. Since the voltage drop is proportional to the charging current, the voltage drop effect will degrade the system capacity significantly when the charging current is relatively large [7]. Moreover, when cells suffer from individual state-of-health (SoH) degradations, they have different ESRs and thus different voltage drops, which implies cells become unbalanced again when the charging is terminated.

Constant–current constant–voltage (CC–CV) charging is a useful scheme to suppress the voltage drop effect through reducing the charging current to zero asymptotically before the charging is finished [12]. Then, existing decentralized and consensus-based cell-balancing methods can be extended to the CC-CV charging scheme to address voltage swell or voltage drop problems. However, compared with the constant-current (CC) charging, the CC-CV charging scheme prolongs the charging time due to the low currents in the constant-voltage (CV) stage. Moreover, in many applications, e.g., in regenerative braking of electric vehicles [13], the charging current is time-varying and determined by road conditions and driving styles, which implies that the CC-CV charging cannot be applied in these applications.

In this paper, we propose an observer-driven consensus-based cell balancing method for charging supercapacitors with various charging profiles. We design a switching Luenberger observer to estimate the voltage of the ESR and the equivalent capacitor of each cell, where the capacitor voltage is further used in the cell-balancing charging control. A consensus-based switching control is designed to charge and balance supercapacitors. Consensus investigates the convergence of a group of agents to a common value through local information exchange with neighbors [15], [16]. In this paper, a three-layer cyber-physical charging system is developed, where the physical layer characterizes the cells and the charging circuit, and the cyber layer represents the communication interactions among cells. In the control layer, the Luenberger observer and consensus-based switching controller are designed for each cell.

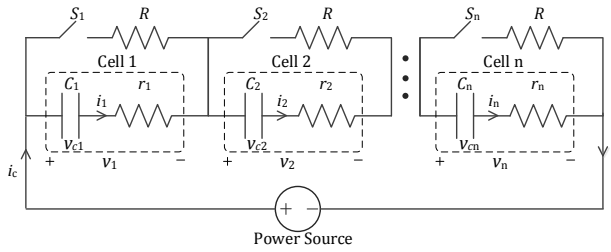

Fig. 1. The switched resistor circuit to charge n cells

The contributions of this paper are threefold.

- We analyze the limitations of existing decentralized method and consensus-based method in voltage swell and voltage drop problems, and suggest the remedy.
- A consensus-based observer-driven charging method is proposed to suppress the voltage swell and voltage drop effects, and the stability of the closed-loop system is rigorously proved.
- Experiment results verify the proposed charging method can alleviate the voltage swell and voltage drop effects with various charging profiles when compared with existing methods.

The remainder of this paper is organized as follows. The modeling and motivation are presented in Section II. In Section III, we propose an observer-driven charging method. A case study is provided in Section IV. The paper is concluded in Section V.

II. System Modeling and Motivation

In this section, we introduce the system modeling and the motivation of this work.

A. System Modeling

1) Physical Modeling: The switched resistor circuit is chosen as the cell balancing circuit due to its popularity in market [7]. In the switched resistor circuit, each cell k is connected with a balancing resistor R through a switch S_k, as shown in Fig. 1. The supercapacitor cell is modeled as a series RC circuit, where the ESR r_k dominates the power loss effect and the equivalent capacitor C_k represents the energy storage effect during the charging process.

The voltage dynamics of the equivalent capacitor C_k are denoted as

$$\dot{v}_{ck} = \frac{i_k}{C_k}, \quad k = 1, \cdots, n \tag{1}$$

where v_{ck} is the voltage of the equivalent capacitor of cell k, C_k is the capacitance of cell k, and i_k is the charging current flowing through cell k, which is computed as

$$i_k = i_c - \frac{v_k}{R} s_k, \tag{2}$$

and i_c is the charging current from the external power source, R is the balancing resistance, s_k represents the binary state of switch k, i.e., $s_k = 0$ means that switch k is off and $s_k = 1$

This article has been accepted for publication in a future issue of this journal, but has not been fully edited. Content may change prior to final publication. Citation information: DOI 10.1109/TII.2019.2935246, IEEE Transactions on Industrial Informatics

implies that switch k is on; v_k is the terminal voltage of cell k, which is derived as

$$v_k = v_{ck} + i_k r_k, \tag{3}$$

and r_k is the ESR of cell k.

The charging current i_c can be constant or time-varying depending on the application scenario. In the CC charging stage, the charging current is a constant specified by the designer. In some applications, e.g., in the regenerative braking of electric vehicles, the charging current is time-varying but the current value is still available with onboard energy management systems [14].

Substituting (2) to (3) yields

$$v_k = \frac{R}{R + s_k r_k} v_{ck} + \frac{R r_k}{R + s_k r_k} i_c. \tag{4}$$

Combining (4) and (3) with (1), we derive the voltage dynamics of cell k as

$$\dot{v}_{ck} = -\frac{s_k}{C_k (R + s_k r_k)} v_{ck} + \frac{R}{C_k (R + s_k r_k)} i_c. \tag{5}$$

Now, we find that both the state equation (5) and output equation (4) have two subsystems depending on the switch state s_k. This implies that the physical system is a switched system, where s_k is the switching signal. Switched systems are a class of hybrid systems, which consist of a group of subsystems along with a switching signal governing the switching among them [17]. By formulating (4) and (5) as a switched linear system, we derive the physical model of cell k in the state space form as

$$\begin{cases} \dot{x}_k = A_k^{\sigma_k} x_k + B_k^{\sigma_k} u, \\ y_k = C_k^{\sigma_k} x_k + D_k^{\sigma_k} u, \end{cases} \tag{6}$$

where state variable $x_k = v_{ck}$ is the voltage of the equivalent capacitor, control input $u = i_c$ is the charging current, output variable $y = v_k$ is the terminal voltage of cell k; $\sigma_k = s_k + 1 \in \{1, 2\}$ is a piecewise constant determining which subsystem is activated; the system parameters for the first subsystem $\Sigma_k^1 = (A_k^1, B_k^1, C_k^1, D_k^1)$ and the second system $\Sigma_k^2 = (A_k^2, B_k^2, C_k^2, D_k^2)$ are defined respectively as

$$A_k^1 = 0, \quad B_k^1 = \frac{1}{C_k}, \quad C_k^1 = 1, \quad D_k^1 = r_k, \tag{7}$$

and

$$\begin{aligned} A_k^2 &= -\frac{1}{C_k (R + r_k)}, & B_k^2 &= \frac{R}{C_k (R + r_k)}, \\ C_k^2 &= \frac{R}{R + r_k}, & D_k^2 &= \frac{R r_k}{R + r_k}. \end{aligned} \tag{8}$$

Then the switched system (6) can be characterized by a sequence of subsystems Σ_k^1 and Σ_k^2 depending on the switching signal $\sigma_k = 1$ or $\sigma_k = 2$. As the stability of the switched system (6) is concerned, the first priority is to determine which switching sequence can stabilize the closed-loop system. We have the following lemma about the stability of the switched system.

Lemma 1 The switched system characterized by (6) for any cell k can be stabilized and cell voltage x_k converges to $x_0 = i_c R$ asymptotically if the switching sequence is chosen as

$$\sigma_k(t) = 2, \quad \forall x_k(t) \geq x_0. \tag{9}$$

Proof. When $\sigma_k(t) = 2$, from (8), we have $A_k^2 < 0$, which means that the closed-loop system is asymptotically stable. From (6) and (8), we can find the only equilibrium for the second subsystem Σ_k^2 is $x_k = x_0$. Thus if we set $\sigma_k(t) = 2$ when $x_k(t) \geq x_0$, the closed-loop system is stable and the state x_k converges to x_0 asymptotically. □

Lemma 1 implies that if the cell voltage is larger than x_0, the second subsystem Σ_k^2 should be activated so that the cell voltage x_k is stabilized to the desired voltage $x_0 = i_c R$. Lemma 1 is useful in analyzing the stability of the developed charging system in Section III.

2) Cyber Modeling: The supercapacitor cells can be mapped as a graph (υ, ε) in the cyber layer, where the node set υ represents the set of cells $1, \cdots, n$ in the circuit, and the edge set ε represents the communication links among cells. Specifically, node 0 is an abstract node, which is called the pinner, representing the reference information to cells and does not correspond to any physical cells.

The graph (υ, ε) can be mathematically characterized by graph matrices. We first define the adjacency matrix $\mathbf{A} = [a_{km}]_{n \times n}$, where $a_{km} = 1$ if there is a directed link from cell m to cell k, i.e., cell m is a neighbor of cell k, and $a_{km} = 0$ otherwise. The degree matrix $\mathbf{D} = \mathrm{diag}(d_k)_n$ is a diagonal matrix, where d_k is the number of neighbors of cell k. Then the Laplacian matrix $\mathbf{L}$ is defined as [18]

$$\mathbf{L} = \mathbf{D} - \mathbf{A}, \tag{10}$$

where the sum of each row of $\mathbf{L}$ is zero. The Laplacian matrix characterizes the communication interactions among cells, i.e., the availability of neighbors' information to cells.

The interactions between the pinner and the cells are characterized by the pinning matrix $\mathbf{G}$, which is defined as

$$\mathbf{G} = \mathrm{diag}(g_k)_n, \tag{11}$$

where $g_k = 1$ if the pinner pins to cell k directly, and $g_k = 0$ otherwise. The pinning matrix characterizes the accessibility of the pinner to cells.

The interactions between the pinner and the cells as well as those among cells can be systematically characterized by graph matrices $\mathbf{L}$ and $\mathbf{G}$. In order to guarantee the synchronization of cell voltages, it is assumed that the pinner pins to at least one cell, and there is a directed spanning tree among cells, where the pinned cell is the root. It is shown that if this condition holds, the matrix $\mathbf{L} + \mathbf{G}$ is positive definite [15].

B. Motivation

Cell imbalance is typically caused by individual cell parameters, e.g., capacitance, ESR, and self-discharge rate [7]. The capacitance is a dominant factor that affects the balancing of supercapacitors during the charging process. ESRs have a critical influence on the voltage drop effect of cells when the

This article has been accepted for publication in a future issue of this journal, but has not been fully edited. Content may change prior to final publication. Citation information: DOI 10.1109/TII.2019.2935246, IEEE Transactions on Industrial Informatics

charging is terminated and the charging current falls to zero. The self-discharge rate or the leakage effect becomes obvious with a long duration in the static setup, e.g., $5\%-15\%$ voltage decay was observed within 48 h after charging [19]. Thus, the dynamic operation of cells is mainly affected by the variations of capacitances and ESRs.

The decentralized cell balancing method has the drawback of large voltage swells during the charging process. Consensus-based methods supplement the decentralized method by synchronizing cell voltages and reducing the voltage swells. However, existing methods still suffer from the voltage drop effect when the charging is terminated. This is because the ESRs are neglected in the cell balancing design, implying cell voltages are less than the desired voltage when the charging is complete. Moreover, when cells suffer from manufacturing tolerance and uneven SoH degradations, cells typically have individual ESRs, which leads to different voltage drops. Then, the capacity of the energy storage system is dominated by the cell with the lowest voltage, which will reduce the available capacity of the energy storage system.

In the following, we provide an experimental measurement to illustrate the effect of ESRs on cell voltages when the charging is terminated, as shown in Fig. 2. We consider the commercially available supercapacitor DMHA14R5V353 with different SoHs, where the rated voltage is 4.5 V and the nominal ESR is $0.3\,\Omega$. In the experiment, three cells are connected in series and are charged with the constant current $i_c = 2$ A. The SoHs of three cells are estimated according to [10]. When terminal voltages of cells reach the rated voltage, the charging is terminated and the charging current falls from 2 A to zero immediately. From Fig. 2, we find that cells have different voltage drops due to the individual ESRs, which further results in the unbalanced cell voltages. The experiment results are summarized in Table I.

TABLE I
SUMMARY OF EXPERIMENT RESULTS IN FIG. 2

Metric\Cell No.	Cell 1	Cell 2	Cell 3
SoH	95%	73%	26%
ESR (Ω)	0.3	0.4	0.55
Voltage Drop (V)	0.6	0.8	1.1
Cell Voltage (V)	3.9	3.7	3.4

From Table I, we have two observations. First, ESRs lead to voltage drop effects when the charging is terminated, which means that cell voltages are less than the desired voltage (4.5 V). Second, individual ESRs result in different voltage drops, implying that cells are unbalanced when the charging is terminated. As shown in Table I, cell 1 has the highest voltage (3.9 V) and cell 3 has the lowest voltage (3.4 V). But the capacity of the energy storage system is dominated by cell 3 for the discharging has to be terminated when cell 3 falls below the safety threshold. This implies that the capacity of the energy storage system will be degraded.

To address this challenge, it is necessary to consider the effect of ESRs by estimating the capacitor voltage x_k during the charging process. Then, a state feedback controller can be designed to balance x_k instead of terminal voltage y_k.

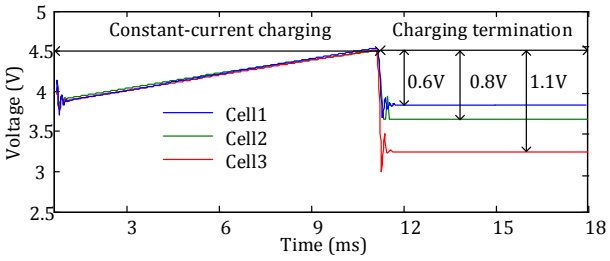

Fig. 2. The effect of ESRs on cell voltages when charging is terminated

If the capacitor voltage x_k is balanced, cell voltages will maintain balanced when the charging is terminated since the capacitor voltage cannot change dramatically with the charging current. In what follows, we will design an observer-driven state feedback control to achieve this objective.

III. Observer-Driven Charging Control

In this section, we propose an observer-driven consensus-based charging method for supercapacitors. We first design a switching Luenberger observer to estimate the system state. Then a state feedback charging control is proposed using a consensus protocol. The closed-loop model of the system is derived and the stability of the closed-loop system is analyzed.

A. Observer Design

We design a switching Luenberger observer to estimate the state x_k based on the output y_k for each cell k. By analyzing properties of the switched system (6), we have the following two important observations.

- The state of the switched system is continuous for any control input, i.e., the state does not jump at the switching instants.
- For any $\sigma_k \in \{1, 2\}$, the σ_kth subsystem is observable.

The first observation is straight-forward since the capacitor voltage x_k cannot change dramatically with the charging current. The second observation holds due to the non-zero scalar $C_k^{\sigma_k}$ in (7) and (8). Then we can design a switching Luenberger observer consisting of two sub-observers based on $\sigma_k \in \{1, 2\}$. The sub-observer for the σ_kth subsystem of cell k is designed as

$$\begin{cases} \dot{\hat{x}}_k = A_k^{\sigma_k}\hat{x}_k + B_k^{\sigma_k}u + \zeta_k^{\sigma_k}\left[y_k - \hat{y}_k\right], \\ \hat{y}_k = C_k^{\sigma_k}\hat{x}_k + D_k^{\sigma_k}u, \end{cases} \tag{12}$$

where $\hat{x}_k$, $\hat{y}_k$ are the estimations of x_k, y_k respectively, and $\zeta_k^{\sigma_k}$ is the observer gain.

The design task is to determine the observer gain $\zeta_k^{\sigma_k}$ that guarantees the estimation $\hat{x}_k$ converges to x_k asymptotically. The estimation error is defined as

$$e_k = \hat{x}_k - x_k. \tag{13}$$

Considering the plant dynamics (6) and the observer dynamics (12), we derive the the observer estimation error dynamics as

$$\dot{e}_k = \bar{A}_k^{\sigma_k} e_k, \tag{14}$$

This article has been accepted for publication in a future issue of this journal, but has not been fully edited. Content may change prior to final publication. Citation information: DOI 10.1109/TII.2019.2935246, IEEE Transactions on Industrial Informatics

where the state matrix $\bar{A}_k^{\sigma_k}$ is represented as

$$\bar{A}_k^{\sigma_k} = A_k^{\sigma_k} - \zeta_k^{\sigma_k} C_k^{\sigma_k}. \tag{15}$$

Now, the observer design problem is converted to guaranteeing the stability of switched linear system (14). The following lemma is useful in analyzing the stability of error system (14).

Lemma 2 [20] For the error dynamics (14), assume for any $\sigma_k \in \{1, 2\}$, $\bar{A}_k^{\sigma_k}$ is Hurwitz and $\bar{A}_k^{\sigma_k} = \bar{A}_k^{\sigma_k T}$, then the error dynamics (14) is globally exponentially stable for arbitrary switching if the state of (14) is continuous.

The continuity of e_k is guaranteed by the continuous state x_k and its estimation $\hat{x}_k$. For the scalar $\bar{A}_k^{\sigma_k}$, $\bar{A}_k^{\sigma_k} = \bar{A}_k^{\sigma_k T}$ holds naturally. Lemma 2 implies that if we can choose $\zeta_k^{\sigma_k}$ that guarantees $\bar{A}_k^{\sigma_k}$ is Hurwitz, i.e., each sub-observer is stable, the stability of the switching observer can be ensured. We will determine $\zeta_k^{\sigma_k}$ using the frequency response method in Section IV.

B. Charging Control

The charging control objective is to ensure that the capacitor voltage x_k tracks the desired voltage x_0 so that the cell voltage can stay at x_0 when the charging is complete. However, the capacitor voltage x_k cannot be measured directly. With observer (12), we can obtain the estimation of x_k in real time. Then, we can use $\hat{x}_k$ in the charging control design.

Now, we need to design a feedback control law to guarantee $\hat{x}_k$ tracks the reference x_0. For a stand-alone cell, the controller typically takes the feedback from the reference x_0 to $\hat{x}_k$. However, for a supercapacitor storage system with multiple cells, it is necessary to consider both the accessibility of the reference x_0 and the availability of neighbors' information to cells. Thus, the tracking error for each cell is designed as

$$\delta_k = g_k \left(x_0 - \hat{x}_k\right) + \sum_{m \in N_k} a_{km} \left(\hat{x}_m - \hat{x}_k\right), \tag{16}$$

where x_0 is the desired voltage, $\hat{x}_k$ is the estimation of x_k, $\hat{x}_m$ is the estimation of x_m, and x_ms are the voltages of cell k's neighbors.

The voltage tracker (16) is a consensus protocol, where the first term guarantees $\hat{x}_k$ converges to x_0, and the second term achieves the voltage synchronization between cell k and its neighbors. Then, a switching control law is designed as

$$\sigma_k = \text{sign}(\delta_k), \tag{17}$$

where the switching logic $\text{sign}(\cdot)$ is defined as

$$\text{sign}(\delta_k) = \begin{cases} 2, & \forall \delta_k \leq 0 \\ 1, & \text{otherwise} \end{cases} \tag{18}$$

In the following theorem, we will prove that the proposed switching control law can stabilize the capacitor voltage x_k to the reference x_0 for any cell $k \in \upsilon$.

Theorem 1 The supercapacitor storage system characterized by (6) can be stabilized by switching law (17) and cell voltages x_k converge to the reference voltage x_0 asymptotically for any cell $k \in \upsilon$ if the following conditions hold:

- The reference pins to at least one cell, and the pinned cell is the root for the spanning tree among cells;
- The observer gain $\zeta_k^{\sigma_k}$ is chosen that the error dynamics (14) is asymptotically stable.

Proof. Define the collective vector form of state $\mathbf{X}$, state estimation $\hat{\mathbf{X}}$, reference $\mathbf{X_0}$, tracking error $\boldsymbol{\Delta}$, and switching signal $\boldsymbol{\sigma}$, respectively, by

$$\begin{aligned} \mathbf{X} &= \begin{bmatrix} x_1 & x_2 & \cdots & x_n \end{bmatrix}^T, \\ \hat{\mathbf{X}} &= \begin{bmatrix} \hat{x}_1 & \hat{x}_2 & \cdots & \hat{x}_n \end{bmatrix}^T, \\ \mathbf{X}_0 &= \begin{bmatrix} x_0 & x_0 & \cdots & x_0 \end{bmatrix}^T, \\ \boldsymbol{\Delta} &= \begin{bmatrix} \delta_1 & \delta_2 & \cdots & \delta_n \end{bmatrix}^T, \\ \boldsymbol{\sigma} &= \begin{bmatrix} \sigma_1 & \sigma_2 & \cdots & \sigma_n \end{bmatrix}^T. \end{aligned} \tag{19}$$

The tracking error (16) can be further written as

$$\begin{aligned} \delta_k &= g_k x_0 - g_k \hat{x}_k + \sum_{m \in N_k} a_{km} \hat{x}_m - \sum_{m \in N_k} a_{km} \hat{x}_k \\ &= -\left(d_k + g_k\right) \hat{x}_k + g_k x_0 + \sum_{m \in N_k} a_{km} \hat{x}_m. \end{aligned} \tag{20}$$

We derive the collective form of the tracking error (20) as

$$\begin{aligned} \boldsymbol{\Delta} &= -\left(\mathbf{D} + \mathbf{G}\right) \hat{\mathbf{X}} + \mathbf{G}\mathbf{X}_0 + \mathbf{A}\hat{\mathbf{X}} \\ &= -\left(\mathbf{D} - \mathbf{A}\right) \hat{\mathbf{X}} + \mathbf{G}\left(\mathbf{X}_0 - \hat{\mathbf{X}}\right) \\ &= -\mathbf{L}\hat{\mathbf{X}} + \mathbf{G}\left(\mathbf{X}_0 - \hat{\mathbf{X}}\right) \end{aligned} \tag{21}$$

It can be found that $\mathbf{L}\mathbf{X}_0 = \mathbf{0}_{n \times 1}$ since the row sum of the Laplacian matrix is zero, which leads to

$$\boldsymbol{\Delta} = \mathbf{L}\mathbf{X}_0 - \mathbf{L}\hat{\mathbf{X}} + \mathbf{G}\left(\mathbf{X}_0 - \hat{\mathbf{X}}\right) = \left(\mathbf{L} + \mathbf{G}\right)\left(\mathbf{X}_0 - \hat{\mathbf{X}}\right). \tag{22}$$

When the reference pins to at least one cell, and the pinned cell is the root for the spanning tree among cells, the matrix $\mathbf{L} + \mathbf{G}$ is positive definite and thus invertible [15]. Thus, we have

$$\boldsymbol{\Delta} \leq \mathbf{0} \Rightarrow \mathbf{X}_0 - \hat{\mathbf{X}} \leq \left(\mathbf{L} + \mathbf{G}\right)^{-1} \mathbf{0} \Rightarrow \mathbf{X}_0 - \hat{\mathbf{X}} \leq \mathbf{0}. \tag{23}$$

Following the switching logic in (18), we have

$$\boldsymbol{\sigma} = \mathbf{2}, \quad \hat{\mathbf{X}} \geq \mathbf{X}_0. \tag{24}$$

Then from Lemma 1, we know that the closed-loop system is stable and the voltage estimation $\hat{\mathbf{X}}$ converges to the desired voltage $\mathbf{X}_0$ asymptotically.

Next, we will prove that the cell voltage $\mathbf{X}$ will converge to $\mathbf{X_0}$. If the observer gain $\zeta_k^{\sigma_k}$ is chosen that the error dynamics (14) is asymptotically stable, from Lemma 2, we have $\mathbf{X} = \hat{\mathbf{X}}$ in the steady state. Then, from (24) and Lemma 1, we know that the cell voltage $\mathbf{X}$ will converge to the desired voltage $\mathbf{X_0}$. This completes the proof. □

From (22), we can find that, with the given switching control law (17) and assuming the error dynamics (14) is stable, the charging control law is only determined by the graph matrices $\mathbf{L}$ and $\mathbf{G}$, which are independent of the physical configuration. This fact implies that the physical configuration of cells will not affect the controller design.

In the proof of Theorem 1, the matrix-vector notation is used due to the interactions among cells in the cyber layer. In the following, we will derive the closed-loop system model using the matrix-vector representation.

This article has been accepted for publication in a future issue of this journal, but has not been fully edited. Content may change prior to final publication. Citation information: DOI 10.1109/TII.2019.2935246, IEEE Transactions on Industrial Informatics

C. Closed-Loop Modeling

In order to obtain the closed-loop model of the supercapacitor system, we first rewrite the switched system (6) in the collective form as

$$\begin{aligned}\dot{\mathbf{X}} =&\mathbf{A}^{\boldsymbol{\sigma}}\mathbf{X}+\mathbf{B}^{\boldsymbol{\sigma}}u,\\ \mathbf{Y} =&\mathbf{C}^{\boldsymbol{\sigma}}\mathbf{X}+\mathbf{D}^{\boldsymbol{\sigma}}u,\end{aligned} \tag{25}$$

where $\mathbf{Y}$ is the collective form of y_k:

$$\mathbf{Y} = \begin{bmatrix} y_1 & y_2 & \cdots & y_n \end{bmatrix}^T, \tag{26}$$

and the matrices are defined as

$$\begin{aligned}\mathbf{A}^{\boldsymbol{\sigma}} &= \mathrm{diag}(A_k^{\sigma_k})_n, \quad \mathbf{B}^{\boldsymbol{\sigma}} = \mathrm{diag}(B_k^{\sigma_k})_n,\\ \mathbf{C}^{\boldsymbol{\sigma}} &= \mathrm{diag}(C_k^{\sigma_k})_n, \quad \mathbf{D}^{\sigma} = \mathrm{diag}(D_k^{\sigma_k})_n.\end{aligned} \tag{27}$$

The collective dynamics of the switching observer (12) can be derived similarly as

$$\begin{aligned}\dot{\hat{\mathbf{X}}} =&\mathbf{A}^{\boldsymbol{\sigma}}\hat{\mathbf{X}}+\mathbf{B}^{\boldsymbol{\sigma}}u+\boldsymbol{\zeta}^{\boldsymbol{\sigma}}\left[\mathbf{Y}-\hat{\mathbf{Y}}\right],\\ \hat{\mathbf{Y}} =&\mathbf{C}^{\boldsymbol{\sigma}}\hat{\mathbf{X}}+\mathbf{D}^{\boldsymbol{\sigma}}u,\end{aligned} \tag{28}$$

where $\hat{\mathbf{Y}}$ is the collective form of $\hat{y}_k$:

$$\hat{\mathbf{Y}} = \begin{bmatrix} \hat{y}_1 & \hat{y}_2 & \cdots & \hat{y}_n \end{bmatrix}^T, \tag{29}$$

and the matrix $\boldsymbol{\zeta}^{\boldsymbol{\sigma}}$ is defined as

$$\boldsymbol{\zeta}^{\boldsymbol{\sigma}} = \mathrm{diag}(\zeta_k^{\sigma_k})_n. \tag{30}$$

Now, we derive the closed-loop model using the block diagram, where the signals represent the variable vectors, and the blocks represent the operation laws of the vectors. We first determine the signals, and then we connect the blocks along the signal flow.

The input signal is the reference $\mathbf{X_0}$, and the output signal is the terminal voltage $\mathbf{Y}$. We can compute the estimation of capacitor voltage $\hat{\mathbf{X}}$ based on the observer block (28). Then the state estimation $\hat{\mathbf{X}}$ is used as the feedback state in the control loop. From (22), we know that the feedback error $\mathbf{X_0} - \hat{\mathbf{X}}$ is injected into the cyber block $\mathbf{L}+\mathbf{G}$ to generate the tracking error $\boldsymbol{\Delta}$, which is further transmitted to the switching control block (17) to generate the switching signal $\boldsymbol{\sigma}$. The switching signal $\boldsymbol{\sigma}$ is injected into the physical block (25) to produce the output $\mathbf{Y}$ and into the observer block (28) to produce the output estimation $\hat{\mathbf{Y}}$. The feedback error $\mathbf{Y_0} - \hat{\mathbf{Y}}$ is fed into the observer gain block $\boldsymbol{\zeta}^{\boldsymbol{\sigma}}$ to generate a bias term, which is transmitted to the observer block (28) to guarantee $\hat{\mathbf{X}} = \mathbf{X}$. In addtion, the charging current u acts as an input to the physical block (25) and observer block (28). Connecting the blocks according to the signal flow, we derive the closed-loop system model, which is shown in Fig. 3.

From the cyber-physical perspective, the closed-loop system can be divided into three layers, i.e., a physical layer, a cyber layer, and a control layer. The physical layer corresponds to the physical block (25) and the cyber layer corresponds to the cyber block $\mathbf{L}+\mathbf{G}$. The control layer is comprised of the control block (17), the observer block (28), and the observer gain block $\boldsymbol{\zeta}^{\sigma}$.

From the above analysis, we know that with the given physical and cyber layer models, the performance of the closed-loop system is determined by the control layer. More specifically, with the designed control block (17) and observer block (28), the system performance is dominated by the observer gain $\boldsymbol{\zeta}^{\boldsymbol{\sigma}}$. In what follows, we will provide a numerical case study to illustrate how to choose the observer gain.

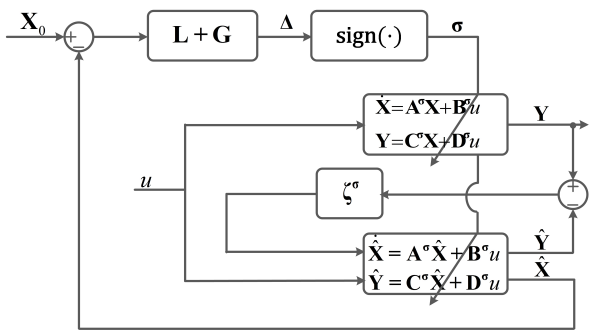

Fig. 3. The closed-loop model of the cyber-physical supercapacitor charging system

IV. Case Studies

In this section, we evaluate the performance of the proposed cell-balancing charging method with a practical case study. We first introduce the parameter setting and the hardware setup. Then, experiments are conducted to verify the effectiveness and superiority of the observer-driven charging method.

A. Parameter Setting

1) Scenario: We consider a supercapacitor energy storage system with three cells which have undergone severe SoH degradations. We assume cell 1 has reached its end-of-life (EoL) and has been replaced with a new cell of the same type. Thus, there are SoH differences between cells 1 and cell 2, 3, i.e., their capacitances and ESRs are different. The parameters of the three cells are given as follows. The capacitances of three cells C_1 = 130 F, C_2 = 122 F, C_3 = 119 F, the ESRs of three cells r_1 = 0.1 Ω, r_2 = 0.13 Ω, r_3 = 0.17 Ω, the initial voltages of three cells $v_1(0) = 0.3$ V, $v_2(0) = 0.4$ V, $v_3(0) = 0.5$ V, the desired voltage of each cell: $v_0 = 2$ V, the resistance of each resistor $R = 2\,\Omega$, switching frequency f_s = 100 Hz.

2) Physical Parameters: From the physical model (6) in Section II-A1, we know that the physical model of each cell k has two subsystems Σ_k^1 and Σ_k^2. The model parameters can be computed based on (7) and (8). Specifically, the model parameters of subsystem Σ_k^1 are calculated as A_1^1 = A_2^1 = A_3^1 = 0, B_1^1 = 0.007, B_2^1 =B_3^1 = 0.008, C_1^1 = C_2^1 = C_3^1 = 1,D_1^1 = 0.1, D_2^1 = 0.13, D_3^1 = 0.17, and the parameters of subsystem Σ_k^2 are calculated as A_1^2 = -0.006, A_2^2 = A_3^2 = -0.007, B_1^2 = 0.006, B_2^2 = B_3^2 = 0.007, C_1^2 = 0.9, C_2^2 = 0.88, C_3^2 = 0.85, D_1^2 = 0.09, D_2^2 = 0.12, D_3^2 = 0.15.

3) Cyber Parameters: From Theorem 1, we know that the communication topology should contain a spanning tree, where the pinned cell is the root. We assume cell 1 is the root and has directed links to cells 2 and 3, and the reference pins to three cells. Then, the graph matrices $\mathbf{L}$ and $\mathbf{G}$ are given by

This article has been accepted for publication in a future issue of this journal, but has not been fully edited. Content may change prior to final publication. Citation information: DOI 10.1109/TII.2019.2935246, IEEE Transactions on Industrial Informatics

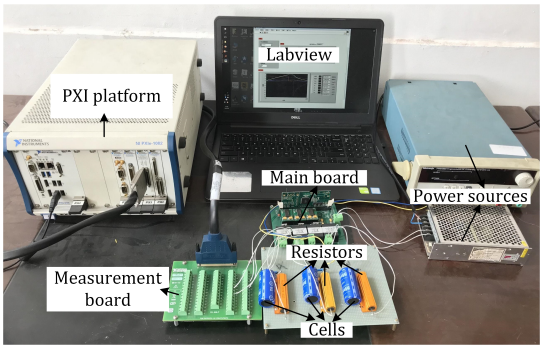

Fig. 4. The experiment setup of the supercapacitor charging system

$$\mathbf{L} = \begin{bmatrix} 0 & 0 & 0 \\ -1 & 1 & 0 \\ -1 & 0 & 1 \end{bmatrix}, \mathbf{G} = \begin{bmatrix} 1 & 0 & 0 \\ 0 & 1 & 0 \\ 0 & 0 & 1 \end{bmatrix}.$$

4) Control Parameters: From Theorem 1, we know that the observer gain $\zeta_k^{\sigma_k}$ should be chosen that the error dynamics (14) is stable. From Lemma 2, it can be found that if $\bar{A}_k^{\sigma_k}$ is Hurwitz, the closed-loop system (14) is stable. Thus, we have

$$\bar{A}_k^{\sigma_k} = A_k^{\sigma_k} - \zeta_k^{\sigma_k} C_k^{\sigma_k} < 0. \tag{31}$$

Now, we will determine $\zeta_k^{\sigma_k}$ using the frequency response method. The Laplace transform of (14) is derived as

$$sE_k(s) - E_k(0) = \bar{A}_k^{\sigma_k} E_k(s), \tag{32}$$

where $E_k(s)$ and $E_k(0)$ are the Laplace transform and initial state of $e_k(t)$, respectively.

It follows from (32) that

$$E_k(s) = \frac{1}{s - \bar{A}_k^{\sigma_k}} E_k(0). \tag{33}$$

Accordingly, the bandwidth of the first-order system (33) is computed as [21]

$$f_b = \frac{\bar{A}_k^{\sigma_k}}{2\pi}. \tag{34}$$

For a practical switched mode power source, we typically choose the bandwidth as $1/10 \sim 1/100$ of the switching frequency. By considering the transient response and robustness of the system, we choose the bandwidth as $1/50$ of the switching frequency. Then, we have

$$\bar{A}_k^{\sigma_k} = -2\pi \tfrac{1}{50} f_s = -12.6.$$

Then, based on (15), the observer gain can be computed as

$$\zeta_k^{\sigma_k} = \frac{A_k^{\sigma_k} - \bar{A}_k^{\sigma_k}}{C_k^{\sigma_k}}. \tag{35}$$

Based on (35), we calculate the observer gain as $\zeta_1^1 = \zeta_2^1 = \zeta_3^1 = 12.6$, $\zeta_1^2 = 12.85$, $\zeta_2^2 = \zeta_3^2 = 12.98$. The effectiveness of the observer gains will be verified with experiment results in what follows.

B. Hardware Setup

Fig. 4 shows the hardware setup of the supercapacitor charging system, which is built based on the schematic in Fig. 1. The laboratory testbed is comprised of a main board, three supercapacitor cells, two power sources, and a PCI eXtensions for Instrumentation (PXI) platform. The main components of the testbed are introduced as follows.

- Main board. The main board consists of a TMS320F2808 micro-processor, three high-precision dividers acting as voltage sensors, three switches of type IRF530 MOSFET, a low-pass filter chip TL074ID, a PWM opto-coupler/driver TLP700A, and a voltage conversion chip PDUKE-24S05.
- Supercapacitor cells. Three supercapacitor cells are connected in series, where each cell is connected in parallel with a resistor through the corresponding IRF530 switches. The parameters of three cells are given in Section IV-A1.
- Power sources. There are a DC 24 V power source and a constant-current power source. The DC 24 V power source supplies the operating voltage for the main board, and the constant-current power source supplies the charging current for the supercapacitors.
- PXI platform. The PXI platform collects cell voltages through the measurement board, and stores the data with LabVIEW® in the hosting computer. PXI is a high-performance and low-cost deployment platform for industrial applications [22].

The experiment process is described as follows. We designed three control procedures (i.e., controllers) in the TMS320F2808 micro-processor, i.e., each controller is responsible for the corresponding cell. Each controller utilizes a high-precision voltage divider to measure the corresponding cell's voltage, which is further filtered by the low-pass filter TL074ID. The controllers communicate with their neighbors based on the specified communication topology in Section IV-A3. With the local measurements and the voltage information received from neighbors, each controller computes the switching signals based on the programmed control law. The PWM signals are generated based on the switching signals to regulate the on/off of switches IRF530 MOSFETs through the PWM optocoupler/driver TLP700A. The TMS320F2808 micro-processor has been programmed and debugged with the Code Composer Studio (CCS) in the hosting computer. The time interval between experiments is set as 10 min for the sufficient cooling down of cells and balancing resistors.

C. Experiment Results

We conduct experiments to compare the cell balancing performance of (i) decentralized method (DM), (ii) consensus-based method (CM), and (iii) observer-driven consensus-based method (OCM). In order to compare the performance of these methods fairly, two different conditions are considered, i.e., charging current $i_c = 1$ A and charging current $i_c = 2$ A. In the performance evaluation, the voltage swell ratio is defined as the voltage deviation divided by the desired voltage, and

This article has been accepted for publication in a future issue of this journal, but has not been fully edited. Content may change prior to final publication. Citation information: DOI 10.1109/TII.2019.2935246, IEEE Transactions on Industrial Informatics

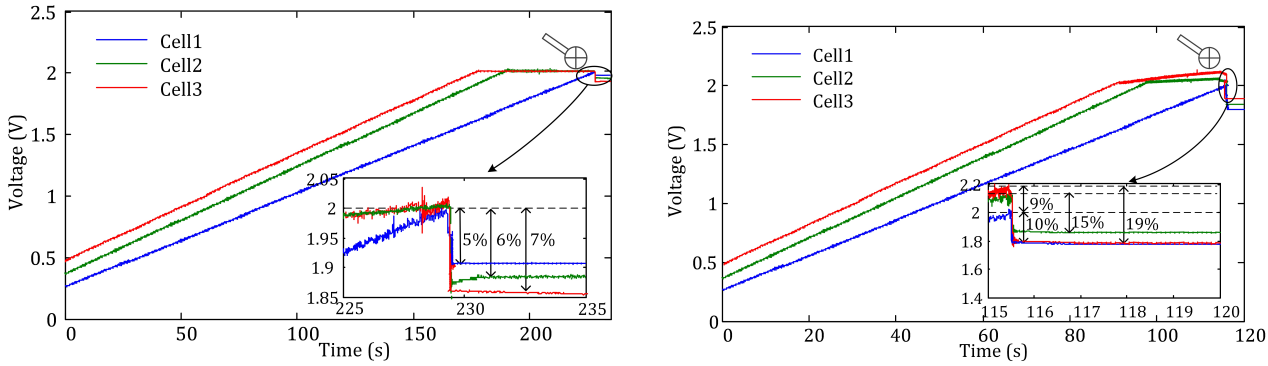

(a) $i_c = 1\,\text{A}$ (b) $i_c = 2\,\text{A}$

Fig. 5. The charging profiles of the decentralized method (DM) with charging current (a) $i_c = 1\,\text{A}$ and (b) $i_c = 2\,\text{A}$

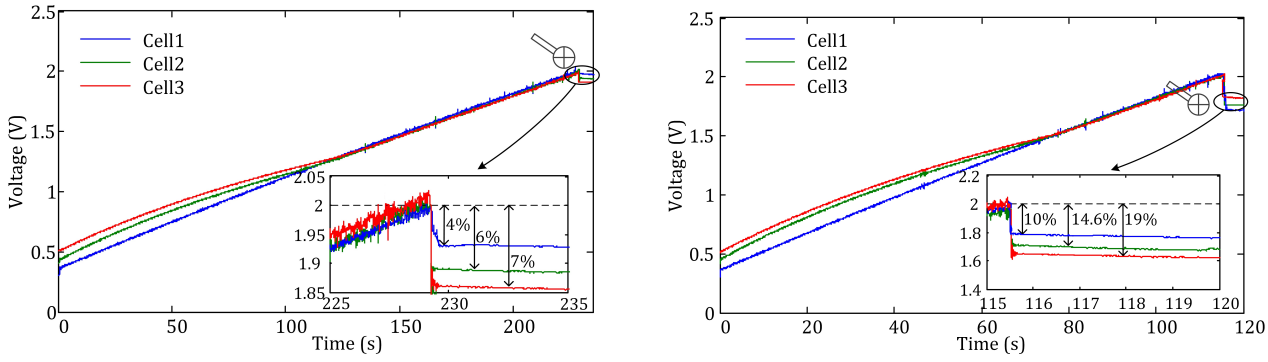

(a) $i_c = 1\,\text{A}$ (b) $i_c = 2\,\text{A}$

Fig. 6. The charging profiles of the consensus-based method (CM) with charging current (a) $i_c = 1\,\text{A}$ and (b) $i_c = 2\,\text{A}$

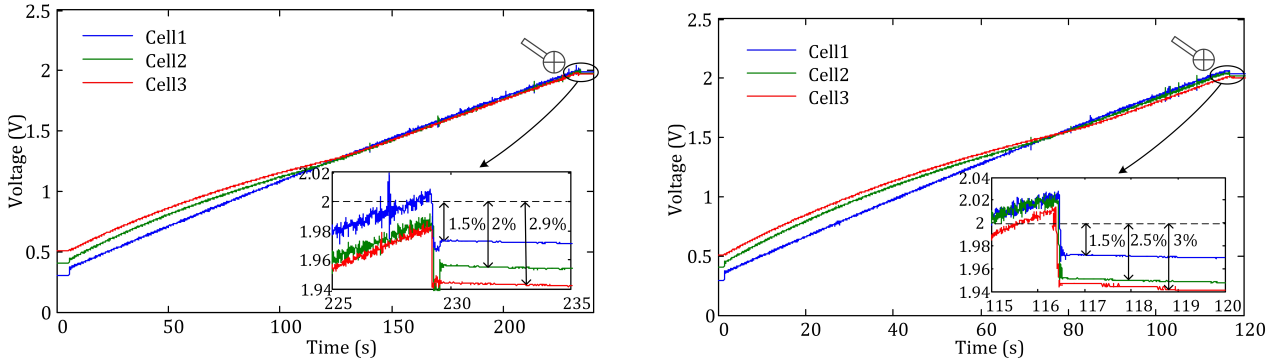

(a) $i_c = 1\,\text{A}$ (b) $i_c = 2\,\text{A}$

Fig. 7. The charging profiles of the observer-driven consensus-based method (OCM) with charging current (a) $i_c = 1\,\text{A}$ and (b) $i_c = 2\,\text{A}$

the voltage drop ratio is defined as the voltage drop divided by the desired voltage.

1) Decentralized Method (DM): Fig. 5 shows the experiment results of the decentralized method (DM) with different charging currents. Fig. 5(a) shows the charging profiles of the DM with $i_c = 1\,\text{A}$. Three cells are charged independently until the cells are fully charged and the charging is terminated around 229 s. As can be seen in Fig. 5(a), three cells suffer from the voltage drop effect due to the ESRs, where the voltage drop ratios of three cells are 4%, 6%, and 7%, respectively. Fig. 5(b) shows the charging profiles of the DM with $i_c = 2\,\text{A}$, where cells suffer from both voltage swells during the charging process and voltage drops when the charging is terminated. The maximum voltage swell ratio is 9%, and the voltage drop ratios of three cells are 10%, 14.6%, and 19%.

By comparing the experiment results of Fig. 5(a) with Fig. 5(b), two phenomena can be observed: (i) cells suffer from voltage swells with $i_c = 2\,\text{A}$, and (ii) the voltage drop increases when charging current increases from $1\,\text{A}$ to $2\,\text{A}$. The first phenomenon can be explained as follows. When a

This article has been accepted for publication in a future issue of this journal, but has not been fully edited. Content may change prior to final publication. Citation information: DOI 10.1109/TII.2019.2935246, IEEE Transactions on Industrial Informatics

cell, e.g., cell 3, is fully charged to the desired voltage 2 V, the switch is turned on and the current flowing through the balancing circuit is $i_R = v_3/R = 1\,\text{A}$. Since the charging current is $i_c = 2\,\text{A}$, the current flowing through cell 3 is $i_3 = i_c - i_R = 1\,\text{A}$, i.e., the charging current is not zero and cell 3 will be overcharged. For the second phenomenon, as the voltage drop is equal to the ESR multiplied by the charging current, the voltage drop increases proportionally with the charging current.

2) Consensus-Based Method (CM): Fig. 6 shows the experiment results of the consensus-based method (CM) with different charging currents. Fig. 6(a) shows the charging profiles of the CM with $i_c = 1\,\text{A}$. It can be found that three cells are fully charged around 229 s, and then the charging is terminated and the charging current decreases to zero. The charing termination leads to the voltage drops of three cells due to the existences of ESRs. The voltage drop ratios of three cells are 4%, 6%, and 7%. Fig. 6(b) shows the charging profiles of the CM with $i_c = 2\,\text{A}$, where the cells are fully charged and the charging is terminated around 115.5 s. The voltage drop ratios of three cells are 10%, 14.6%, and 19%.

By comparing the voltage drop ratios of the corresponding cell in Fig. 6(a) and Fig. 6(b), we can find that the voltage drop increases with the charging current. This fact implies the CM may suffer from severe voltage drop effects in applications where the charging current is relatively large. Compared with Fig. 5, an advantage of the CM is that it effectively avoids the voltage swells by synchronizing cell voltages during the charging process.

3) Observer-Driven Consensus-Based Method (OCM): Fig. 7 shows the experiment results of the proposed observer-driven consensus-based (OCM) method with different charging currents. Fig. 7(a) shows the charging profiles of the OCM with $i_c = 1\,\text{A}$. It can be found that three cells are fully charged around 229 s. The voltage drop ratios of three cells are 1.5%, 2%, and 2.9%. Fig. 7(b) shows the charging profiles of the OCM with $i_c = 2\,\text{A}$, where the cells are fully charged around 115.5 s. The voltage drop ratios of three cells are 1.5%, 2.5%, and 3%.

By comparing the experiment results of Fig. 6(a)(b) with Fig. 7(a)(b), respectively, we can find that the proposed method can effectively suppress the voltage drops of cells when the charging is terminated. Moreover, the proposed method provides a comparable voltage drop suppression performance when the charging current increases from 1 A to 2 A. By comparing the experiment results of Fig. 5(b) with Fig. 7(b), we can find the proposed OCM can also suppress the voltage swells effectively during the charging process. The maximum voltage drop of the three methods with different charging currents are summarized in Table II.

TABLE II
THE MAXIMUM VOLTAGE DROP OF THE THREE METHODS

	DM	CM	OCM
$i_c = 1\,\text{A}$	7%	7%	2.9%
$i_c = 2\,\text{A}$	19%	19%	3%

From Table II, we can find the proposed OCM is effective in suppressing the voltage drop effect in both $i_c = 1\,\text{A}$ case (2.9% vs. 7%) and $i_c = 2\,\text{A}$ case (3% vs. 19%) when compared with the existing methods.

D. Further Discussions

1) Practicality: In the proposed model-based observer, the ESR values are required. The ESRs can be measured offline using a constant-current charging test. If the charging current is I_R, and the voltage step (during charging startup) or voltage drop (during charging termination) is ΔV, the ESR can be computed as $\Delta V/I_R$ [23]. The ESRs can also be estimated online using online identification algorithms, e.g., recursive least square (RLS) algorithm [24].

2) Energy Efficiency: The energy efficiency of the supercapacitor energy storage system is defined as the stored energy in cells divided by the input energy from the external power source, i.e.,

$$\phi = \frac{E_{stg}}{E_{chg}}, \tag{36}$$

where ϕ is the energy efficiency, E_{stg} is the stored energy in cells, and E_{chg} is the input energy from power sources.

Based on the RC model of supercapacitors, we compute the stored energy E_{stg} during the charging process as [8]

$$E_{stg} = \frac{1}{2}\sum_{k=1}^{n} C_k\big[x_k(T)^2 - x_k^2(0)\big], \tag{37}$$

where T is the charging time, $x_k(T)$ is the equivalent capacitor voltage of cell k when the charging is complete, and $x_k(0)$ is the initial voltage of cell k.

The input energy E_{chg} from the external power source during the charging process is derived as

$$E_{chg} = \sum_{k=1}^{n}\int_0^T v_k(\tau) i_c \mathrm{d}\tau, \tag{38}$$

where $v_k(\tau)$ is the terminal voltage of cell k.

When cells are charged with the constant current, the input energy is further computed as

$$E_{chg} = i_c\sum_{k=1}^{n}\int_0^T v_k(\tau)\mathrm{d}\tau = u\sum_{k=1}^{n}\int_0^T y_k(\tau)\mathrm{d}\tau. \tag{39}$$

Based on (36) and the charging profiles in Fig. 5–Fig. 7, we can compute the energy efficiencies of the DM, CM, and OCM, which are summarized in Table III.

TABLE III
THE ENERGY EFFICIENCY OF THE THREE METHODS

	DM	CM	OCM
$i_c = 1\,\text{A}$	73.2%	83.4%	87.6%
$i_c = 2\,\text{A}$	68.9%	74.5%	87.5%

From Table III, we can find the energy efficiency of the proposed OCM is superior to existing methods. This is because the OCM can effectively suppress the voltage drop, which implies more energy can be stored. Moreover, for the DM and CM, the energy efficiency decreases as the current increases

This article has been accepted for publication in a future issue of this journal, but has not been fully edited. Content may change prior to final publication. Citation information: DOI 10.1109/TII.2019.2935246, IEEE Transactions on Industrial Informatics

from 1 A to 2 A. This is because with the increase of current, the voltage drop becomes obvious and the stored energy gets smaller. By contrast, the energy efficiency of the OCM is roughly the same with different charging currents due to the voltage drop suppression.

3) SoH Variations: One advantage of supercapacitors is that their lifetime is relatively long, and thus their degradations can only be observed in the long-term operation. However, with existing SoH degradation formulas [10] and the parameter setting in Section IV-A, it is still possible to emulate the SoH degradations of cells through the repeated charging simulations. Fig. 8 shows the simplified emulation for SoH degradations of three cells under the proposed method with i_c =2 A and temperature 25°C. From the conceptual emulation in Fig. 8, we can find that cells with smaller SoHs degrade faster. This is because that cells with smaller SoHs typically suffer from a relatively larger SoH loss due to the accelerated aging effect during each charging cycle.

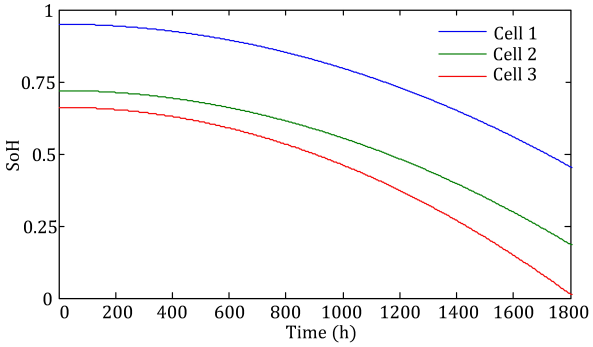

Fig. 8. The SoH variation of three cells under the proposed method with i_c=2 A and temperature 25°C

4) Dynamic Charging Profile: Fig. 9 shows the experiment results of the proposed OCM under dynamic charging profiles. As shown in Fig. 9(a), cells are first charged with current 1 A until 115 s, and are further charged with 2 A from 115 s to 150 s. From 150 s to 180 s, cells are charged with 1 A again, and the charging current falls to zero after 180 s. The voltage profiles of three cells are shown in Fig. 9(b), where we can see cell voltages are synchronized around 100 s. When the charging current increases from 1 A to 2 A, the voltage slope increases. When the charging is terminated around 180 s, the maximum voltage drop is about 3%, which conforms well with Fig. 7(a). These facts imply that the proposed method is still effective with dynamic charging profiles.

5) CC-CV Charging Profile: The CC-CV charging is another useful scheme to suppress the voltage drop effect by reducing the charging current during the CV stage. As shown in Fig. 10, we extend existing DM and CM to the CC-CV charging mode, where three cells are first charged with a constant current 2 A and then with a constant voltage 6 V. Fig. 10(a) depicts the experiment results of the DM with CC-CV charging. It can be found cell 3 suffers from voltage swells (5%) due to the resistance deviation caused by thermal effects. But the maximum voltage drop decreases considerably (5% vs 19%) when compared with DM under CC charging

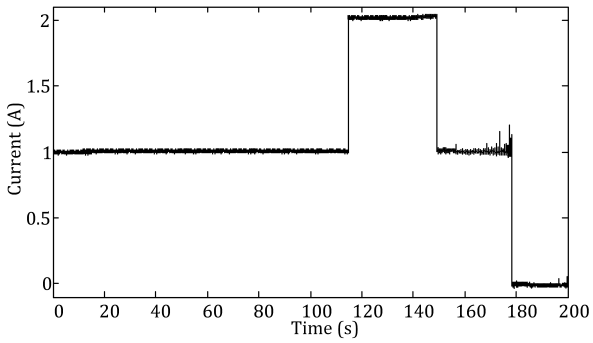

(a) Current Profile

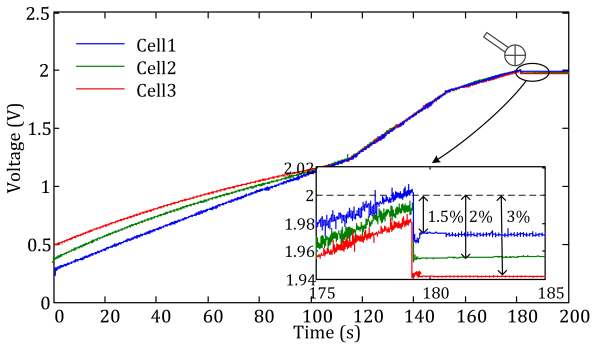

(b) Voltage Profile

Fig. 9. The experiment results of the proposed OCM with dynamic charging profiles

in Fig. 5(b). The experiment results of the CM with CC-CV charging are shown in Fig. 10(b), where we find cell voltages are synchronized around 80 s and voltage swells are avoided. The CM with CC-CV charging provides a better voltage drop suppression performance (2% vs 19%) than the CM with CC charging in Fig. 6(b). Although the CC-CV charging provides a comparable voltage drop suppression (2% vs 3%) compared with the proposed OCM, there are two deficiencies of the CC-CV charging. First, by comparing Fig. 5(b), Fig. 6(b) with Fig. 10(a), Fig. 10(b), we can find the charging time of the CC-CV scheme is significantly prolonged. Second, in many applications, e.g., in the regenerative braking of EVs, the charging profile is determined by operation conditions, which implies that the CC-CV charging cannot be applied.

6) Cost: In small-scale energy storage systems, the communications among cells in the cyber layer do not necessarily introduce additional hardware cost. In this paper, cells are directly connected to a micro-controller, where cells are mapped as nodes in the cyber layer. Thus the communication links are nothing more than the signal flows in the software design. Then, the proposed method has no extra hardware cost when compared with the existing methods. In large-scale energy storage applications, however, geographically-distributed micro-controllers may be deployed. In this case, additional communication hardware is required to transmit information among micro-controllers. But since the proposed charging method is a distributed approach, a sparse communication topology can satisfy the requirement.

This article has been accepted for publication in a future issue of this journal, but has not been fully edited. Content may change prior to final publication. Citation information: DOI 10.1109/TII.2019.2935246, IEEE Transactions on Industrial Informatics

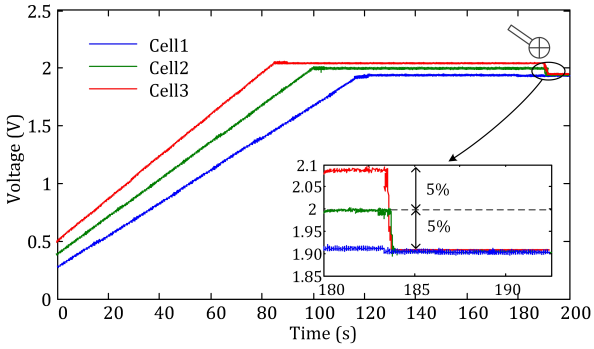

(a) DM

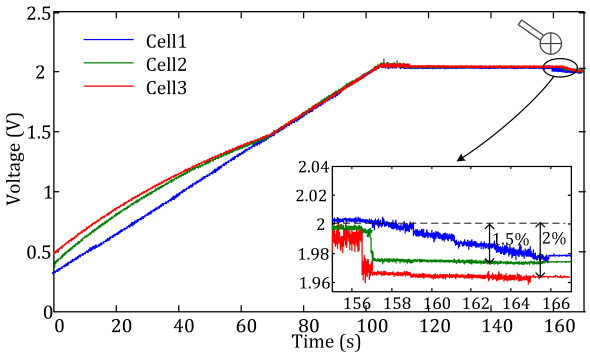

(b) CM

Fig. 10. The charging profiles of (a) DM and (b) CM under CC-CV charging scheme

7) Scalability: The proposed charging method is a distributed control approach, i.e., each controller only uses the neighboring information to compute the control input. This implies the proposed method benefits from a good scalability, i.e., the design complexity will not increase with the number of cells. Thus the proposed charging method is applicable to large-scale supercapacitor energy storage systems with many cells.

V. Conclusion

In this paper, we proposed an observer-driven charging method for supercapacitors with the aim of suppressing both voltage swells during charging process and voltage drops during charging termination. We first analyze the limitations of existing methods. Then, we propose an observer-driven consensus-based charging method, where a switching Luenberger observer and a consensus-based switching controller are designed, respectively. The closed-loop system model of the charging system is developed using the block diagram. Experiment results show that the proposed method is effective in alleviating voltage swells and voltage drops of supercapacitors as intended. In the future work, we will further explore the cell balancing of supercapacitors with model-free observers.

References

[1] C. Zou, L. Zhang, X. Hu, Z. Wang, T. Wik, M. Pecht, "A review of fractional-order techniques applied to lithium-ion batteries, lead-acid batteries, and supercapacitors," *Journal of Power Sources*, vol. 390, pp. 286–296, 2018.

[2] L. Zhang, X. Hu, Z. Wang, F. Sun, and D. G. Dorrell, "A review of supercapacitor modeling, estimation, and applications: A control/management perspective," *Renewable and Sustainable Energy Reviews*, vol. 81, no. 2, pp. 1868–1878, 2017.

[3] Q. Zhang, W. Deng, and G. Li, "Stochastic control of predictive power management for battery/supercapacitor hybrid energy storage systems of electric vehicles," *IEEE Transactions on Industrial Informatics*, vol. 14, no. 7, pp. 3023–3030, 2018.

[4] H. Li, J. Peng, J. He, R. Zhou, Z. Huang, and J. Pan, "A cooperative charging protocol for onboard supercapacitors of catenary-free trams," *IEEE Transactions on Control Systems Technology*, vo. 26, no. 4, pp.1219–1232, 2017.

[5] J. Barreras, D. Frost, D. Howey, "Smart balancing systems: An ultimate solution to the weakest cell problem?" *IEEE Vehicular Technology Society Newsletter*, March 2018.

[6] J. Cao, N. Schofield, and A. Emadi. Battery balancing methods: A comprehensive review. In *2008 IEEE Vehicle Power and Propulsion Conference*, pp. 1–6, 2008.

[7] D. Linzen, S. Buller, E. Karden, and R. W. De Doncker, "Analysis and evaluation of charge-balancing circuits on performance, reliability, and lifetime of supercapacitor systems," *IEEE Transactions on Industry Applications*, vol. 41, no. 5, pp. 1135–1141, 2005.

[8] F. Ibanez, "Analyzing the need for a balancing system in supercapacitor energy storage systems," *IEEE Transactions on Power Electronics*, vol. 33, no. 3, pp. 2162–2171, 2017.

[9] D. F. Frost, and D. A. Howey, "Completely decentralized active balancing battery management system," *IEEE Transactions on Power Electronics*, vol. 33, no. 1, pp. 729–738, 2018.

[10] S. Shili, A. Hijazi, A. Sari, X. Lin-Shi, and P. Venet, "Balancing circuit new control for supercapacitor storage system lifetime maximization," *IEEE Transactions on Power Electronics*, vol. 32, no. 6, pp. 4939–4948, 2017.

[11] H. Li, J. Peng, J. He, Z. Huang, and J. Pan, "Synchronized cell-balancing charging of supercapacitors," *IFAC-PapersOnLine*, vol. 50, no. 1, pp. 3338 – 3343, 2017.

[12] A. B. Khan, W. Choi, "Optimal charge pattern for the high-performance multistage constant current charge method for the Li-Ion batteries," *IEEE Transactions on Energy Conversion*, vol. 33, no. 3, pp. 1132–1140, 2018.

[13] M. Khodaparastan, A. A. Mohamed, W. Brandauer, "Recuperation of regenerative braking energy in electric rail transit systems," *IEEE Transactions on Intelligent Transportation Systems*, to be published.

[14] B. Liu, L. Li, X. Wang, S. Cheng, "Hybrid electric vehicle downshifting strategy based on stochastic dynamic programming during regenerative braking process," *IEEE Transactions on Vehicular Technology*, vol. 67, no. 6, pp. 4716–4727, 2018.

[15] X. Li, X. Wang, and G. Chen, "Pinning a complex dynamical network to its equilibrium," *IEEE Transactions on Circuits and Systems I: Regular Papers*, vol. 51, no. 10, pp. 2074–2087, 2004.

[16] Z. Zuo, Q. Han, B. Ning, X. Ge, and X. Zhang, "An overview of recent advances in fixed-time cooperative control of multiagent systems," *IEEE Transactions on Industrial Informatics*, vol. 14, no. 6, pp. 2322–2334, 2018.

[17] D. Zhai, X. Liu, and Y. J. Liu, "Adaptive decentralized controller design for a class of switched interconnected nonlinear systems," *IEEE Transactions on Cybernetics*, to be published.

[18] D. B. West *et al.*, *Introduction to Graph Theory*. Prentice hall Upper Saddle River, 2001, vol. 2.

[19] M. Kaus, J. Kowal, and D. U. Sauer, "Modelling the effects of charge redistribution during self-discharge of supercapacitors," *Electrochimica Acta*, pp. 55, no. 25, pp. 7516–7523, 2010.

[20] W. Chen and S. Mehrdad, "Observer design for linear switched control systems," in *Proceedings of the 2004 American Control Conference*, vol. 6, pp. 5796–5801, 2004.

[21] R. C. Dorf and R. H. Bishop, *Modern Control Systems*. Pearson, 2011.

[22] "What is PXI?" http://www.ni.com/pxi/whatis/.

[23] N. Devillers, S. Jemei, M. C. Pera, D. Bienaime, F. Gustin, "Review of characterization methods for supercapacitor modelling," *Journal of Power Sources*, vol. 246, pp. 596–608, 2014.

[24] N. Reichbach and A. Kuperman, "Recursive-least-squares-based real-time estimation of supercapacitor parameters," *IEEE Transactions on Energy Conversion*, vol. 31, no. 2, pp. 810–812, 2016.

This article has been accepted for publication in a future issue of this journal, but has not been fully edited. Content may change prior to final publication. Citation information: DOI 10.1109/TII.2019.2935246, IEEE Transactions on Industrial Informatics

Heng Li (M'17) is currently an Assistant Professor in School of Computer Science and Engineering, Central South University, China. He received his Bachelor's degree and PhD degree from Central South University in 2011 and 2017, respectively. From Nov 2015 to Nov 2017, he worked as a research assistant in Department of Computer Science, University of Victoria, Victoria, Canada. His current research interests include cooperative control and energy storage systems.

Jun Peng (M'08) is a Professor in School of Computer Science and Engineering at the Central South of University, China. She received her B.S. degree from Xiangtan University and the MSc degree from National University of Defense Technology, China, in 1987 and 1990, respectively. She received her PhD degree from Central South University in 2005. In April 1990, she joined the staff of Central South University. From 2006 to 2007, she was with School of Electrical and Computer Science of University of Central Florida, USA, as a visiting scholar. Her research interests include cooperative control; cloud computing and wireless communications.

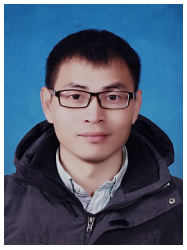

Jianping He (M'15) is currently an Associate Professor in the Department of Automation at Shanghai Jiao Tong University, Shanghai, China. He received the Ph.D. degree in control science and engineering from Zhejiang University, Hangzhou, China, in 2013, and had been a research fellow in the Department of Electrical and Computer Engineering at the University of Victoria, Canada, from Dec. 2013 to Mar. 2017. His research interests mainly include the smart sensing and control, security and privacy theory and applications, distributed learning and big data. He serves as an associate editor for the KSII Transactions on Internet and Information Systems. He was also a guest editor for the International Journal of Robust and Nonlinear Control and Neurocomputing. He received the best paper award of IEEE WCSP'17 and the finalist best student paper award of IEEE ICCA'17.

Zhiwu Huang (M'08) is a Professor in School of Automation at the Central South of University, China. He received his BS degree in Industrial Automation from Xiangtan University in 1987, received his MS degree in Industrial Automation from Department of Automatic Control, University of Science and Technology Beijing in 1989 and received his PhD degree in Control Theory and Control Engineering from Central South University in 2006. In October 1994, he joined the staff of Central South University. From 2008 to 2009, he was with School of Computer Science and Electronic Engineering of University of Essex, U.K., as a visiting scholar. His research interests include fault diagnostic technique and cooperative control. He is a member of IEEE.

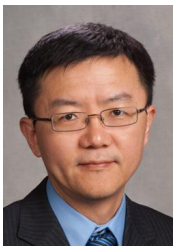

Jing Wang (M'00-SM'11) Jing Wang received his Ph.D. in control theory and control engineering in 1997 from Central South University, China. He was a Postdoctoral Research Fellow at the Institute of Computing Technology, Chinese Academy of Sciences, from 1997 to 1999 and at the Department of Electrical and Computer Engineering, National University of Singapore, from 1999 to 2002. From 2002 to 2007, he was with the School of Electrical Engineering and Computer Science of the University of Central Florida as a Research Assistant Professor. From 2007 to 2014, he was with the Department of Computer Engineering, Bethune-Cookman University, Florida, first as an Assistant Professor and then as a tenured Associate Professor. Since August 2014, he has been with the Department of Electrical and Computer Engineering, Bradley University, Peoria, Illinois. His current research interests include systems and controls, distributed optimization and machine learning, robotics, and control applications.